ADVANCED ENERGY MATERIALS
www.advenergymat.de

Operando Observations of SEI Film Evolution by Mass-Sensitive Scanning Transmission Electron Microscopy

*Chen Hou, Jiuhui Han, Pan Liu, Chuchu Yang, Gang Huang, Takeshi Fujita, Akihiko Hirata, and Mingwei Chen**

The solid electrolyte interphase (SEI) spontaneously formed on anode surfaces as a passivation layer plays a critical role in the lithium dissolution and deposition upon discharge/charge in lithium ion batteries and lithium-metal batteries. The formation kinetics and failure of the SEI films are the key factors determining the safety, power capability, and cycle life of lithium ion and lithium-metal batteries. Since SEI films evolve with the volumetric and interfacial changes of anodes, it is technically challenging in experimental study of SEI kinetics. Here operando observations are reported of SEI formation, growth, and failure at a high current density by utilizing a mass-sensitive Cs-corrected scanning transmission electron microscopy. The sub-nano-scale observations reveal a bilayer hybrid structure of SEI films and demonstrate the radical assisted SEI growth after the SEI thickness beyond the electron tunneling regime. The failure of SEI films is associated with rapid dissolution of inorganic layers when they directly contact with the electrolyte in broken SEI films. The initiation of cracks in SEI films is caused by heterogeneous volume changes of the electrodes during delithiation. These microscopic insights have important implications in understanding SEI kinetics and in developing high-performance anodes with the formation of robust SEI films.

1. Introduction

The solid electrolyte interphase (SEI) is an electronical insulating and ionic conducting microlayer and spontaneously forms on anodes by the reduction of electrolytes in rechargeable lithium ion batteries (LIBs) and lithium-metal batteries.[1–4] The SEI films directly affect the dissolution and deposition of lithium during discharge and charge and thus are one of the key factors that determine the safety, power capability, morphology of lithium deposits, shelf life, and cycle life of LIBs. In particular, the breakdown of SEI can result in the nucleation and growth of lithium dendrites and cause the safety risk for the practical applications of LIBs in the electric vehicles and other high-energy-density electronic devices.[5,6] While, a stable and robust SEI film can effectively inhibit the lithium dendrite growth and thus prominently enhance the cycling performance and safety of the batteries.[1,7] Owing to directly growing on anode surfaces, the formation and stability of SEI films are greatly influenced by the volume variation of anodes during the charge–discharge cycling, especially at a high current density.[1,8] Although the importance of SEI has been widely recognized, the structure and kinetics of SEI are the less well-understood phenomena impacting battery technology. Various in situ techniques, for instances, in situ spectroscopic ellipsometry,[9] in situ nuclear magnetic resonance (NMR),[10] in situ X-ray diffraction,[11] in situ Fourier transform infrared (FTIR) spectroscopy,[12] and in situ electrochemical impedance spectroscopy,[13] have been employed to investigate the evolution of SEI films. Nevertheless, most of them are limited to the non-intuitive investigations. Several key questions on the SEI film formation, structure and failure are still elusive.

Recently, in situ transmission electron microscopy (TEM) has been utilized as a power tool to explore the evolution of SEI films in LIBs. In particular, a liquid cell TEM technique can well mimic the chemical and electrochemical reactions in liquid media with controllable charge and discharge conditions of LIBs. Sacci et al. performed the first in situ TEM observations of SEI film formation on a gold electrode during cyclic voltammetry testing.[14] They found that SEI films form heterogeneously on the gold electrode and possess dendritic morphology. The formation and growth of SEI films on graphite/electrolyte interfaces were studied by Unocic et al. using in situ TEM.[15] By utilizing the liquid cell TEM, Zeng et al. monitored the structural evolution of SEI films in a cyclic voltammetry process and found that the growth of SEI films is limited by the electron transport and produces gaseous

C. Hou, Dr. P. Liu
State Key Laboratory of Metal Matrix Composites
School of Materials Science and Engineering
Shanghai Jiao Tong University
Shanghai 200030, P. R. China

C. Hou, Dr. J. H. Han, C. C. Yang, Dr. G. Huang, Dr. T. Fujita, Dr. A. Hirata, Prof. M. W. Chen
Advanced Institute for Materials Research
Tohoku University
Sendai 980–8577, Japan
E-mail: mwchen@jhu.edu

Prof. M. W. Chen
Department of Materials Science and Engineering
Johns Hopkins University
Baltimore, MD 21214, USA

The ORCID identification number(s) for the author(s) of this article can be found under https://doi.org/10.1002/aenm.201902675.

DOI: 10.1002/aenm.201902675

products by side reactions at the interface between electrode and SEI films.[16] These in situ TEM observations offer microscopic insights into the kinetics of SEI. However, the evolution of SEI films, particularly at high charge rates, have not been fully understood because of insufficient spatial resolution of liquid-cell TEM and the complexity of SEI evolution during charge and discharge. Moreover, possible influence from electron beam irradiation of conventional TEM may also aggravate the complexity of SEI kinetics.

In this study, we conducted operando scanning TEM (STEM) characterization on the evolution of SEI films during lithiation and delithiation at a high charge rate of ≈34C using a lithium ion liquid microcell. The spherical aberration corrected (Cs-corrected) STEM used in this study is equipped with a high angle annular dark-field (HAADF) and an annual bright-field (ABF) detector, which provides sub-nanoscale mass-sensitive contrast to visualize the formation, growth and failure of SEI films. Moreover, the Cs-corrected STEM is operated under low-dose mode to avoid possible influence from electron beam irradiation at a high spatial resolution.

2. Results

Figure 1a,b is schematic diagrams of lithium ion liquid microbattery used for the operando STEM observations. The microbattery is composed of two silicon microchips. The electrochemical chip is patterned with electrodes for performing electrochemical reactions and measurements. The spacer chip is patterned with a 100-nm-thick polymer spacer layer and provides a flowing pathway for the liquid electrolyte (Figure 1a). The gold electrodes patterned on the electrochemical chip are directly connected with an external electrochemical workstation for galvanostatic discharge and charge tests at a constant current of 20 μA, equal to a high charge/discharge rate of ≈34C. The continuously floating electrolyte (see Figure S1 and the Supporting Information) provides the Li ions to the in situ liquid microbattery constantly. Gold is selected as the working electrode because the SEI film formation on gold electrodes has been observed in previous reports[14,16] and gold offers high Z contrast for a better spatial resolution of STEM.[8] Moreover, similar to silicon and lithium anodes, the gold electrodes undergo a vastly volume change during lithiation and delithiation, which gives an opportunity to mimic the evolution of SEI films during large expansion and shrinkage of anodes at a high charge/discharge rate in real LIBs systems. Figure 1c,d present an example that a gold electrode experiences a lithiation–delithiation cycle in the liquid microbattery, evidencing that the gold electrode undergoes a violently volume change during the charge and discharge. After the delithiation, nanosized cracks and voids are all over the entire gold anode (Figure 1d). Figure 1e shows the in situ galvanostatic charge/discharge profiles of the liquid microbattery measured in STEM at the constant current of ≈34C. The cut-off capacity of the operando experiment is 1533 mAh g^{-1}. It has been reported that Li–Au binary system possesses two potential plateaus during Au lithiation and three potential plateaus during Au delithiation.[8] While the charge curve in Figure 1e only presents one potential plateau during the Au lithiation and the discharge curve only presents two potential plateaus during Au delithiaiton. It is probably due to the serious polarization and high overpotential caused by the large current rate used in this study.

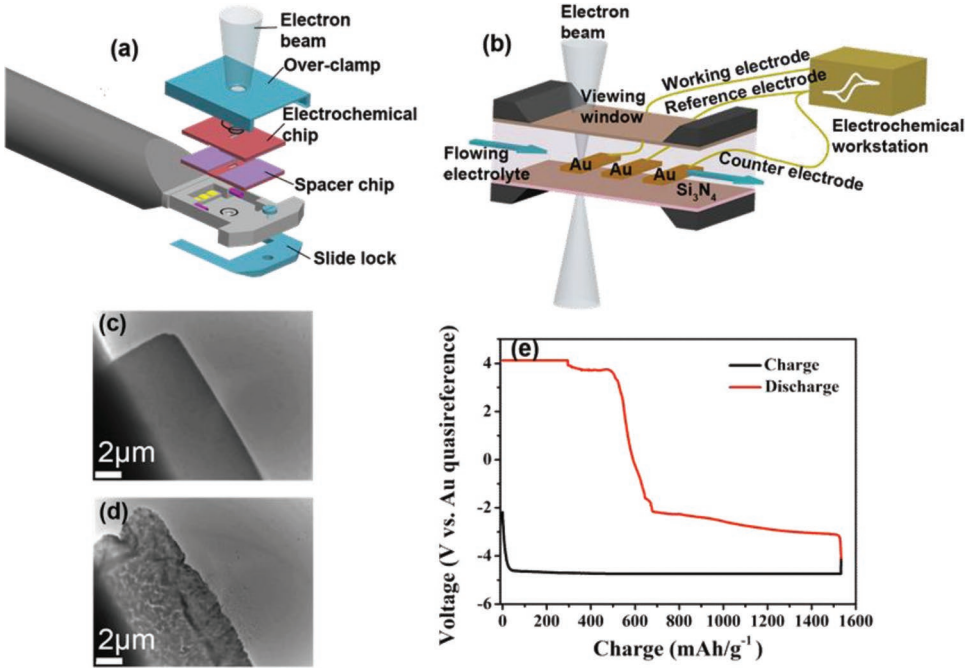

Figure 1. a) Schematic view of lithium microcell setup for operando STEM observations of SEI film evolution and Li–Au reaction. b) The configuration of lithium ion microcell with three electrodes for electrochemical measurements. c) Transmission electron microscopy (TEM) image of a gold anode before charge/discharge testing. d) TEM image of the gold anode after delithiation. e) Galvanostatic discharge/charge profiles measured from the microbattery at a high charge rate of 34C. The cut-off capacity is 1533 mAh g^{-1}.

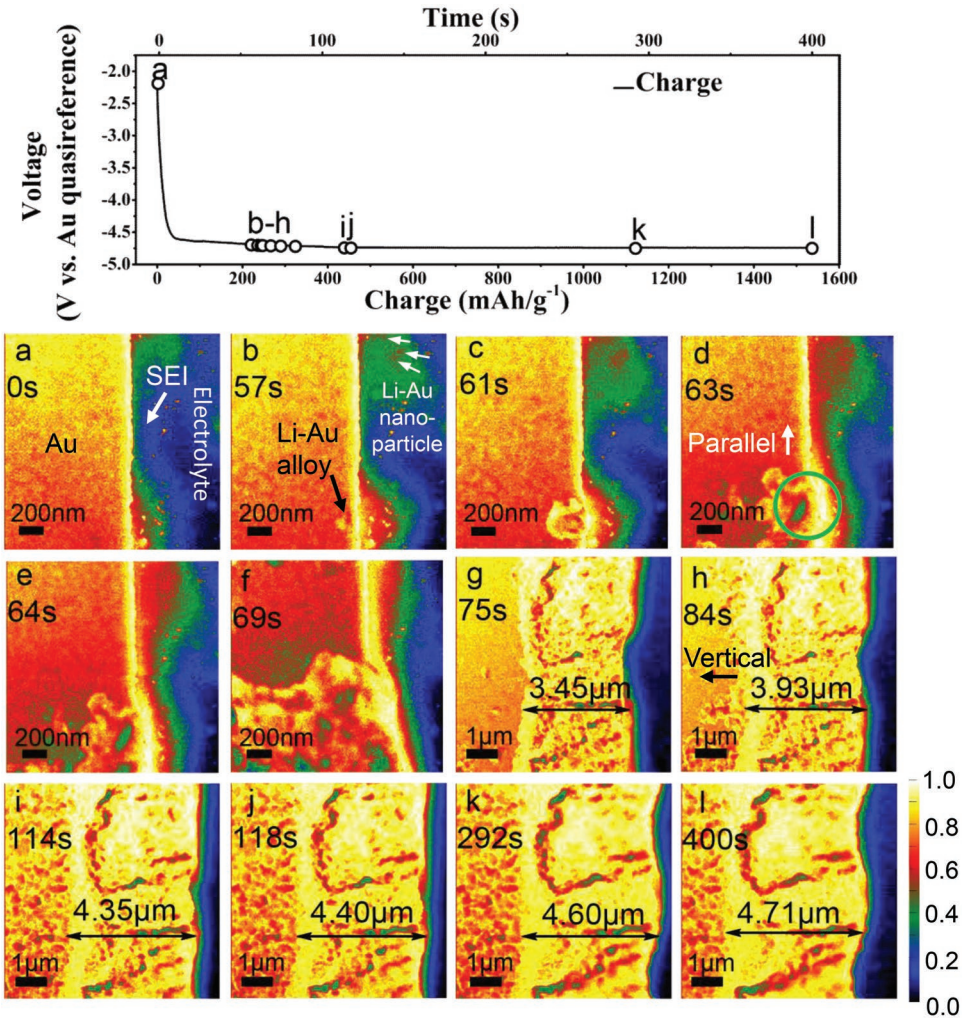

Figure 2. Time sequential HAADF-STEM images of Au lithiation. The charge states of each image are plotted in the charging profile. The temperature colors are configured to enhance the weak Z-contrast of the light SEI film.

HAADF-STEM and ABF-STEM observations with a high spatial resolution are performed to image the SEI film evolution during lithiation and delithiation in real space and real time.

Figure 2 shows the time sequential HAADF-STEM images of SEI film evolution, accompanying with gold lithiation. In comparison with the dark black contrast of the liquid electrolyte, the gold anode and SEI film possess a brighter contrast and can be easily distinguished during the operando observations. The gold anode shows the bright yellow/red color, probably owing to the uneven deposited thickness and heterogeneous microstructure. While the SEI film can be identified as a green color layer. The interface region between the SEI film and electrolyte displays a dark blue contrast, which is probably an assemblage of radical and neutral species that are produced via the initial electrolyte reduction and attracted in the anode surroundings under the applied electric fields.[17] At the initial stage of the lithiation, a SEI layer with inhomogeneous thickness has already formed on the surface of gold anode (Figure 2a), most likely resulting from a quick spontaneous reaction between the gold electrode and the electrolyte since the initial voltage of the liquid cell is –2.18 V versus Au (pseudo) below the reduction potential of the electrolyte (–0.75 V versus Au (pseudo)).[1,8] With continuously charging, the SEI film gradually becomes thick while the Li ions pass through the SEI film and react with the underneath gold electrode. The formation of Li–Au alloy can be recognized from the obvious contrast change and local volume expansion in the region at the interface between the gold electrode and SEI layer, which is marked by the black arrow in Figure 2b. Although the Li ions are too light to be directly seen by the Z-contrast imaging, the formation of Li–Au alloy leads to local intensity variation in the HAADF-STEM images. Note that Li–Au nanoparticles can be observed in the SEI layer at the early stage of charging, as marked by the white arrows in Figure 2b. These trapped Li–Au nanoparticles have different contrast from Au particles (for example in **Figure 3**d) and are probably formed by Au cations that are peeled from the Au cathode during a fast charge process.[18] The SEI film has an uneven thickness and thickness increment even at the initial stage (Figure 2b–d), which is related to the inhomogeneous distribution electric fields around the rough surface of the electrode from heterogeneous microstructure.[3,19–21] Moreover, the distribution of the Li–Au nanoparticles trapped in the SEI film is also inhomogeneous

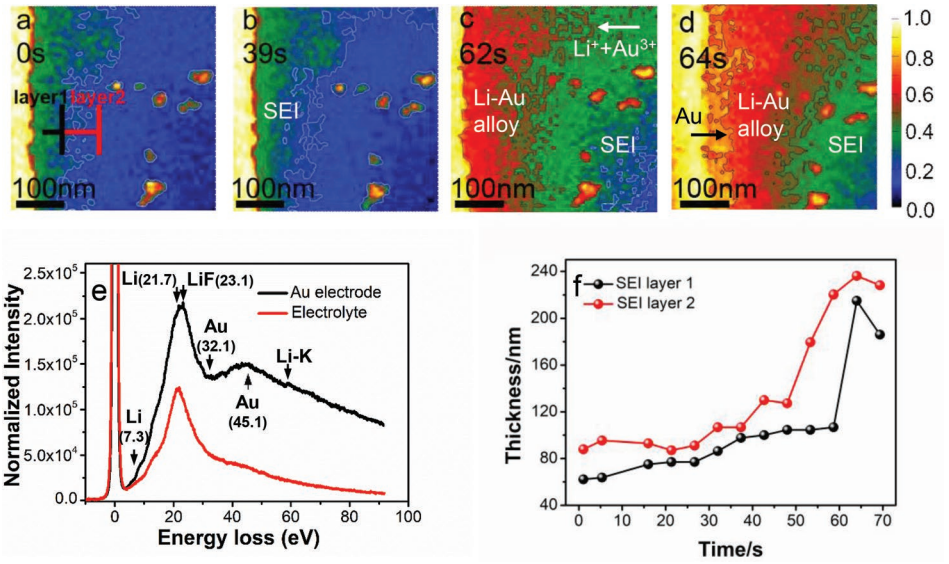

Figure 3. a–d) Time sequential high-magnification HAADF-STEM images of SEI film. The images are zoomed in from Figure 2. e) In situ EELS profiles of the SEI film on the surface of Au electrode and surrounding liquid electrolyte. The spectra were taken at the end of Au lithiation. f)The measured thickness of SEI film as a function of time during Au lithiation process.

and they usually appear in the thick SEI regions where the underneath Au electrode surface is protruding out. As shown in Figure 2c–f, the Li–Au domain grows faster underneath the thinner SEI film region, indicating that thicker SEI suppresses the transportation of Li ions from the electrolyte to the gold anode. The violent deformation and growth of the Li–Au alloy domain result in the formation of voids (or microcracks), which is marked by the green circle in Figure 2d. In contrast, the thickness of the SEI layer becomes more uniform by rapid growth (Figure 2d–f). The zoom-out image (Figure 2g) shows the rapid growth of the Li–Au phase between the SEI film and pure gold. The Li–Au alloy zone has a thickness of about 3.45 µm. Interestingly, at the initial stage of Li–Au phase nucleation, the growth of Li–Au domain is parallel to the electrode/SEI interface (Figure 2c–f), indicating the majority of Li ions come from the nucleation sites which have a thinner SEI layer, rather than from the electrolyte across the thicker SEI regions. With further lithiation and formation of a relatively uniform SEI film, the growth of Li–Au domain changes from the parallel to the vertical directions (Figure 2g,h), indicating that the majority of Li ions for the Li–Au phase formation come from the liquid electrolyte by passing through the SEI film evenly. Meanwhile, the slope of charging curve changes from the short-range diffusion lithiation (about 0.002 V s^{-1}) to the flat long-range diffusion lithiation (about 0.0003 V s^{-1}). Furthermore, the growth rate of the Li–Au alloy domain decreases significantly from ≈149 nm s^{-1} in the range of 57–65 s to ≈4.3 nm s^{-1} in the range of 75–400 s. (see Figure S2a in the Supporting Information). With the lithiation progress, the SEI film continually evolves to be more uniform and smooth and attaches well on the Li–Au electrode surface.

To investigate the structure evolution of the SEI film, Figure 3a–d is the time sequential zoom-in images of the SEI film taken in the first 64 s. The edge of the SEI film is marked by fine white lines to highlighting the contour of the SEI film. According to Figure 3a, the initially formed SEI film possesses a typical double-layer structure, consisting of brighter inorganic inner layer at the electrode surface and relatively dark organic outer layer in the electrolyte side. The contrast of the double-layer SEI film is consistent with previous assumption that the inner layer is comprised of compact inorganic products (e.g., Li_2CO_3, LiF, Li_2O, etc.) with a relatively higher mass density and the outer layer is reduced organic products (e.g., $(CH_2OCO_2Li)_2$, ROLi, $ROCO_2Li$, etc., where R is the alkyl group that depends on the solvent), which has a relatively low density.[1,3,16,22] The obvious contrast variation of the inner layer indicates inhomogeneous density distribution of the inorganic products. During charging the inner layer is continually growing and keeping a rough interface with the organic layer (Figure 3a–d). Additionally, the outer organic layer of the SEI film maintains the porous feature and a rough interface with the electrolyte. Thus, the initial formation of the SEI film on the gold anode appears to take two steps. First, the electrolyte decomposes on gold surface and immediately forms a thin uneven SEI film with porous organic and inorganic layers. Second, the electrolyte permeates into the porous SEI layer to be continually decomposed for the SEI film growth. The growth of the SEI film tends to stop when the inner SEI layer becomes dense and uniform that can prevent electrolyte permeation (Figure S2a, Supporting Information). Again, Li–Au nanoparticles with relatively bright contrast can be observed in the SEI film. Since the bright Li–Au particles appear in the blue zone between SEI and electrolyte, it provides direct evidence that the particles precipitate from the electrolyte. Importantly, the reduction reaction in the electrolyte also indicates that the blue zone indeed enriches with radical species that allows the continuous reduction reaction as well as SEI layer growth after the anode is passivated by the thick and uniform SEI film.[17,23] In order to facilitate the operando observations, the edge of Au electrode and Li–Au alloy zone are highlighted by fine black

and blue lines in Figure 3c,d. The white arrow in Figure 3c represents the diffusion pathway of the Li ions and Au cations and the black arrow in Figure 3d marks the expansion direction of Au electrode during lithiation. Figure 3e shows the electron energy-loss spectroscopy (EELS) spectra of these bright nanoparticles and electrolyte, which were measured during the operando observations. Although these low-energy peaks are broad, the consistence in peak positions with Li,[24] Au,[25] and LiF[26] plasmon peaks and Li–K edge demonstrates that these bright nanoparticles indeed contain Li and Au elements. We also investigated the Li–K edge taken from the inorganic layer of the SEI film. The comparison of the fitted Li–K edge with those of known Li compounds (Figure S3, Supporting Information) confirms that the inorganic layer is a mixture of lithium compounds and the dominant phase appears to be Li carbonate while a small amount of LiF, LiOH, and metallic Li may also exist in the layer. The growth rates of the two distinct layers of the SEI film are plotted in Figure 3f on the basis of the direct observations. Although the data are scattered owing to the rough interfaces and inhomogeneous volume changes of the underneath Au electrode during the heterogeneous Li–Au phase nucleation and growth, the two distinct layers of the SEI film possess a similar growth tendency during the charge process (Figure 3f). The profiles presented in Figure 3f also suggest that the thickness of the SEI film keeps changing with the volume expansion of the gold anode. It is commonly believed that the growth rate of SEI films is controlled by the decomposition rates of electrolytes. From our observations, the growth rate is closely related to the volume changes of the anode as illustrated in Figure S2 in the Supporting Information. The quasi-exponential profile of SEI film growth indicates that the SEI film thickness keeps dynamic changing during charge. At the initial stage, both organic and inorganic layers of the SEI film gradually grow at the nearly same pace. At ≈50 s, the growth rate of SEI film is obviously accelerated. Correspondingly, the gold electrode has an obvious volume expansion with the formation of voids and microcracks. Linking these dots, we can reasonably deduce that the accelerated SEI growth may be associated with the enlarged tensile strains. The severely stretching can promote the transportation of small radicals, such as Li atoms, passing through the SEI films which accelerate the decomposition of the electrolyte. Therefore, the SEI film is not only stretched to be thinner via electrode volume expansion but also continually grows to be thicker via electrolyte reduction even after the thickness is larger than the critical value for electron tunneling.[27] This scenario is supported by the decoupled growth between the organic and inorganic layers in the period between 50–60 s (Figure 3f). The 10 s lag offers direct evidence that the SEI growth takes place at the SEI/electrolyte interface and starts from the organic transformation.[17]

Figure 4 shows that the failure process of the SEI film accompanied with violently shrinkage of gold electrode during the fast discharge at ≈34C. From the initial discharge up to 221 s (Figure 4a,b), the SEI layer maintains as a uniform and continuous film on the anode as viewed from the low-magnification images. Accordingly, the discharge profile remains as a smooth curve with a slight increase of overpotential and the thickness of the Li–Au phase layer gradually decreases for about 15% from 4.71 to 3.98 μm. At 268 s, obvious roughening and swelling of the SEI film take place (Figure 4d), accompanying with significant jump of the overpotential from −2 to about +4 V. In particular, the damage of the SEI layer occurs, which is associated with the surface roughening of the partially delithiated Au at the electrode/electrolyte interface and large volume shrinkage of the gold electrode. The broken SEI film quickly dissolves into the electrolyte and forms a directly contacted interface between the electrolyte and the Au electrode, which could be responsible to the potential jump (Figure 4c–h). Furthermore, the large current rate used in this study may also enlarge the potential jump by increasing the voltage polarization in such microcell system. Fortunately, before the potential over the decomposition voltage of electrolyte (5 V vs Li), the cycle has been finished. The dissolution of the SEI film also leads to rapid delithiation of the Li–Au phase and a sharply shrinkage of the Au electrode in the period from 256 to 277 s (Figure S2b, Supporting Information). Moreover, the dissolution of the inorganic layer of the SEI film (Figure 4h–j) results in the delamination of the entire SEI film from the electrode. Apparently, the failure of the SEI film is initiated by the anode surface roughening and the formation of spike-like delithiated Li–Au phase during the fast discharge and significant volume shrinkage. Especially, the spike-like feature may puncture the SEI film and leads to the fast dissolution of inorganic layers by the direct contact with the electrolyte. The formation of rough spike-like surface is apparently associated with the inhomogeneous volume shrinkage of the electrode and rapid immigration of the electrode/SEI interface. Since the SEI failure mainly takes place during delithiation, the scarcity of radicals, likely Li atoms, for electrolyte reduction and hence SEI self-healing may also play an important role in the failure. After the delithiation reaction, the Au anode has been verified to include the FCC Au and $LiAu_3$ (cP4, $\alpha = 3.97$ Å) two phases by selected area electron diffraction. (Figure S4, Supporting Information)

Since the large mass contrast difference between the Au electrode and the SEI film, the HAADF-STEM cannot properly reveal the detailed structure of the hybrid inorganic-organic SEI film. ABF-STEM has the advantage to image the light elements by partially taking the diffraction contrast together with mass contrast.[28] We conducted an additional operando observations on the evolution of SEI film under ABF-STEM imaging mode and for the first time revealed the kinetic evolution of the organic and inorganic layers, separately. **Figure 5** shows time sequential ABF-STEM images of the morphology variation of the SEI film and interaction between SEI film and intercalated Au electrode at the constant current of ≈34C. The diffraction contrast of ABF-STEM images reveals the polycrystalline structure of the gold electrode with an average grain size of ≈100 nm (Figure 5a). The thickness of the SEI film again is not homogeneous and closely correlated with the heterogeneous nucleation and growth of Li–Au phase (Figure 5b,c), consistent with the HAADF-STEM observations. From the ABF-STEM images, the inhomogeneous lithiation starts from the nucleation with the formation of a Li–Au domain (Figure 5d,e). The large local volume expansion at the Li–Au nucleation site leads to the formation of a V-shape region (Figure 5e,f),[29] which causes the obvious SEI film thinning by stretching and subsequent thickening. **Figure 6** shows the magnified ABF-STEM images of Figure 5. The bilayer

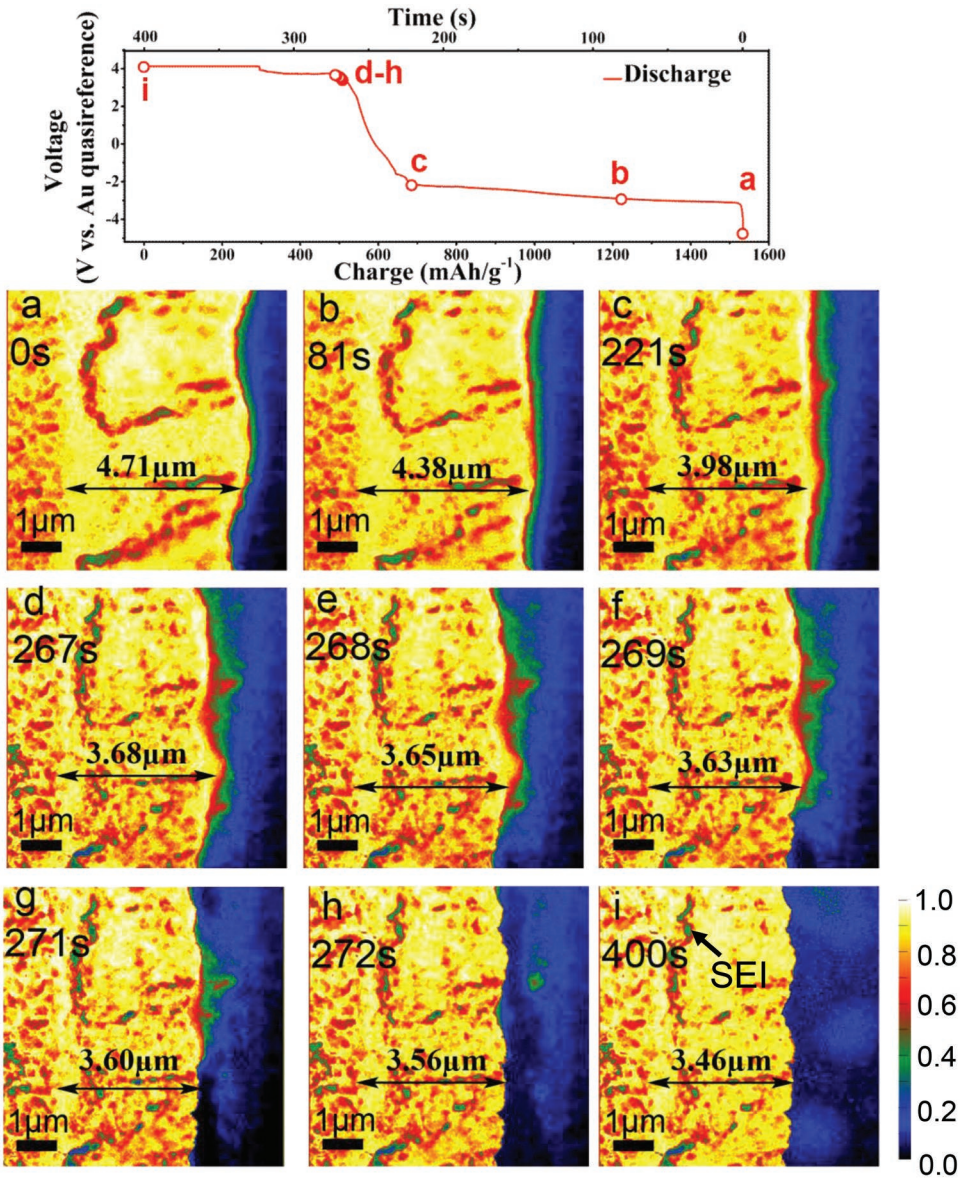

Figure 4. Time sequential HAADF-STEM images during delithiation. The discharge states of each image are plotted in the profile. The temperature colors are configured to enhance the weak Z-contrast of the light SEI film.

structure of the SEI film is clearly visible and highlighted by the red and black fine lines in the inserted image in Figure 6a. As we cannot identify the polycrystalline structure in the inorganic layer from diffraction-contrast ABF-STEM, the SEI layer looks like amorphous in our operando experiment with very limited number of charge/discharge cycling. Again, the thickness of the SEI film is inhomogeneous at the initial stage of lithiation (Figure 6a). The thickness and morphology of the SEI film vary with the contour of the electrode surface, suggesting the inhomogeneity of the SEI film is associated with the surface roughness and, thus, uneven ionic current distribution of the Au electrode. During charging, the evolution of the SEI film echoes with the nucleation and growth of the Li–Au phase (Figure 6a–c). The relation between Li–Au alloy domain development and SEI film growth is shown in Figure S5 in the Supporting Information. The SEI film forms prior to the nucleation of the Au–Li phase and most likely the reduced Li atoms on the surface of the Au anode are directly involved into the nucleation and initial growth of the SEI film. After the nucleation of the Li–Au phase, it grows at a nearly constant rate under the constant current condition. However, the growth of the SEI layer is not smooth but swinging. This can be explained by the alternate switch between the stretch thinning of the SEI film by the volume expansion of the Au–Li phase growth and the stress-assisted rapid growth of the stretched SEI film. The nucleation of the Li–Au phase always takes place at protruding regions of the electrode where a high ionic current is expected. The volume expansion caused by the Li–Au phase growth first makes the SEI film thinner by stretching the film and subsequently local thickening takes place, most

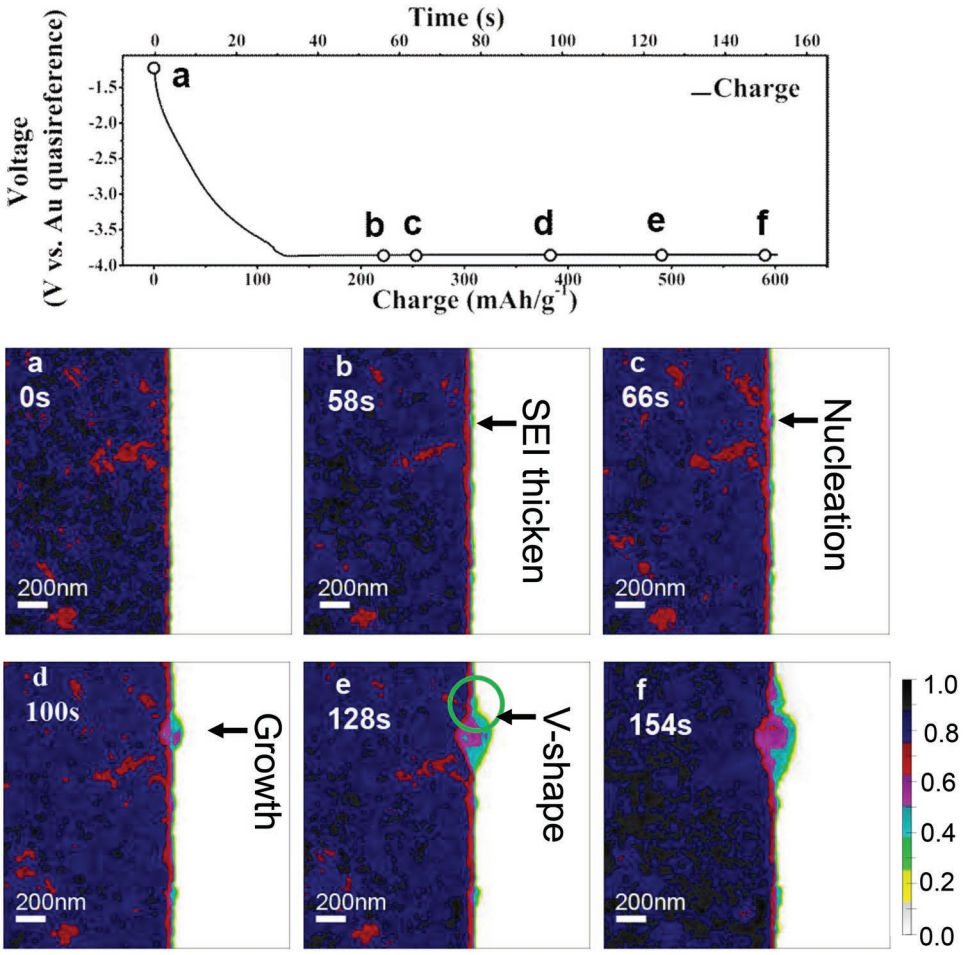

Figure 5. Time sequential ABF-STEM images of Li lithiation. The discharge states of each image are plotted in the galvanostatic charge profile. The zone colors are configured to enhance the weak contrast of the light SEI film. The cut-off capacity is 663 mAh g^{-1}.

likely driven by the stress-assisted SEI growth. The alternative changes in the local thickness results in the heterogeneous SEI film thickness (Figure 6d–f). The thickness changes of the two distinct layers of the SEI film with charging are plotted in Figure 6g. The two layers have a similar growth tendency and undergo the alternating changes between thickening and thinning in accordance with the growth and out-of-plane expansion of the Li–Au phase.

3. Discussion

As it has been widely recognized that the SEI film is one of the most important components but least understood in rechargeable Li batteries, the fundament mechanisms of SEI film formation and failure remain largely unclear with several critical questions unanswered.[3,17,30] The most fundamental question could be the structure of SEI films. For examples,

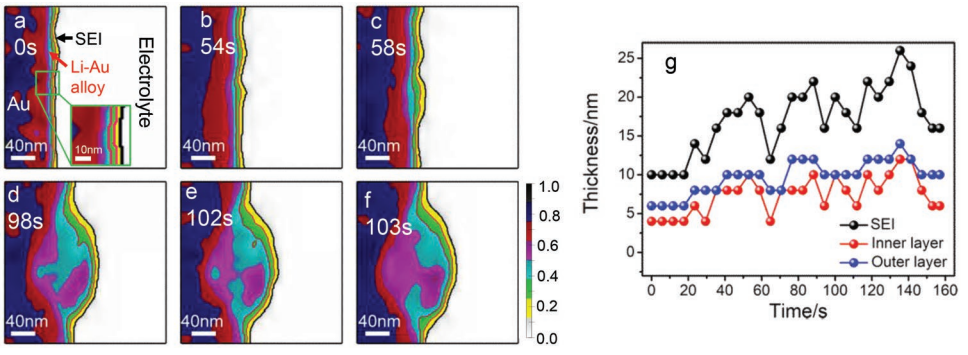

Figure 6. a–f) Time sequential ABF-STEM images of a SEI film, which is zoomed in from Figure 5. The black and red fine lines highlight the bilayers structure of the SEI film. g) The measured thickness of SEI film as a function of time during lithiation.

Peled suggested that the SEI film has an integral structure except for several defects for Li ions migration.[2] Kanamura et al. proposed that the SEI film is a mixture of organic and inorganic deposited phases.[31] Ein-Eli suggested that the SEI film is composed of the lined-up depositions based on a coulombic interaction mechanism.[32] Although the structure of SEI films may vary with compositions of electrolytes, charge/discharge rates, and anode materials, recent experimental results from spectroscopies, such as XPS, suggest that the SEI film has an inorganic/organic bilayer structure which is composed of LiF and Li_2CO_3 close to the electrode surface (inner film) and a porous organic or polymeric layer extending out from the surface (outer film). However, such bilayer structure has not been directly visualized by any imaging techniques during charge and discharge.[3,16,33] By utilizing the mass-contrast of STEM, we provide the direct evidence on the dynamic formation of the bilayer structure of the SEI film. As revealed by our ABF-STEM images (Figure 6), the SEI films have an inner inorganic layer with a relatively bright contrast and an outer layer directly contacting with electrolyte. Since the initial formation of the SEI film on the gold anode, it contains the two distinguished inorganic/organic layers with different contrast in the STEM images. The SEI film grows from an initial porous and uneven inorganic/organic bilayer to a uniform film with a solid inorganic layer and porous organic layer. The change of the bilayer structure leads to the transition of lithiation from the short-range to the long-range diffusion in the charging curve. Moreover, the failure of the SEI film is mainly caused by the rapid dissolution of the inorganic layer after SEI breakdown.

The growth mechanisms of SEI films are also the subject of intense discussion, especially after the film thickness is larger than tens of nanometers and electron tunneling cannot be operated for the reduction of electrolytes.[3,17,34,35] Pinson et al. suggested that the formation of new SEI film takes place between the electrode and SEI films by the slow diffusion of electrolyte molecules through the SEI, which is driven by the concentration gradient between the outer and inner surfaces of SEI.[36] While this model can explain the continuous growth of SEI films without the requirement of tunneling electrons, it is inconsistent with commonly accepted understanding of the organic–inorganic bilayer structure of SEI.[3] In our operando observations, we indeed observed that the penetration of the liquid electrolyte is involved into the SEI growth from a heterogeneous film to a continuous and uniform film through the voids of the films in the initial stage of the SEI formation. In the slow growth process of the uniform SEI film it is not likely that SEI grows via the electrolyte molecule diffusion. In fact, the model is not consistent with the present STEM observations that the SEI thickness evolution takes place by the simultaneous growth of the outer organic and inner inorganic layers (Figure 6g). On the basis of the first-principles calculations, it has recently been suggested that radical species (such as EC- in ethylene carbonate (EC) electrolyte and F- in fluorinated ethylene carbonate (FEC) electrolyte) are responsible for SEI growth when SEI thickness is beyond the electron tunneling regime and solvent penetration.[17] However, this assumption has not been verified by any experiment. In our operando observations, the radical species enriched zone in front of the SEI film has been observed by the mass-sensitive HAADF-STEM image, which displays a dark blue contrast (Figure 2). The charged radicals can cause molecule polarization and local ordering in electric fields and give rise to enhanced contrast from additional electron scattering.[37] Moreover, the precipitation of Li–Au nanoparticles in the dark blue zone provides additional evidence on the existence of negatively charged radicals in the zone, which allows the electron transfer for reduction reactions of the Au and Li ions as well as the electrolytes for continuous SEI growth.

4. Conclusion

In summary, we have systematically investigated the microstructural evolution of SEI films on an Au electrode, together with the voltage and current responses, during lithiation and delithiation at a high charge rate of ≈34C. The mass-sensitive STEM operando characterization reveals the hybrid bilayer structure of SEI films. The simultaneous growths of the inorganic and organic layers provide compelling evidence that the SEI growth take place at the SEI/electrolyte interface by the reduction of electrolytes. Our observations also experimentally demonstrate that the continuous growth of SEI is assisted by radical species that may be formed in the initial stage of charging/discharging and possible diffusion of Li atoms from the anode to the electrolyte. The failure of the SEI films is associated with the repaid dissolution of the inorganic layers after the cracks are generated by heterogeneous volume shrinkage of the electrodes and the scarcity of radicals for electrolyte reduction during discharge. Although these phenomena are observed from a model Li–Au system, they have important implications in elucidating the fundamental mechanisms of SEI kinetics in real Li battery for the development of high-performance Li anodes with stable and robust SEI films.

5. Experimental Section

Li Ions Liquid Microcell Setup and In Situ Electrochemical Measurements: The liquid cell apparatus included two ultrathin silicon chips with the dimensions of 2.6 mm × 3.4 mm × 200 µm and 2.6 mm × 2.6 mm × 200 µm, respectively. The two chips were face-to-face sealed in a TEM liquid-electrochemistry holder (Hummingbird Scientific). The top chip was deposited with three 100-nm-thick and 18-µm-wide gold electrodes which were used as a working electrode (WE), counter electrode (CE), and reference electrode (RE) to constitute a three-electrode cell configuration. The bottom chip had a 100-nm-thick polymer spacer. Both chips have a 50-nm-thick amorphous Si_3N_4 window which is electron transparent for monitoring electrochemical reactions in gold electrodes. In the experiments, the working electrode was used as the anode and the counter electrode as the cathode. 1.0 M $LiPF_6$ EC/DMC (ethylene carbonate/dimethyl carbonate in a 1:1 volume ration) solution was used as the nonaqueous electrolyte feeding into the liquid cell at a low pumping rate of 1 µL min^{-1} by an external syringe and pump device. A thick liquid layer of ≈200 nm was used to minimize possible influence of electrolyte thickness and Si3N4 windows on the kinetics of electrochemical reactions. An electrochemical workstation (IVIUM CompactStat)) was employed to perform the galvanostatic charge/discharge tests at a constant current of 20 µA, which is equal to ≈34C (see the Supporting Information).

Operando STEM Observations of the Li Ions Liquid Microcell: A JEM-2100F TEM (JEOL, 200 keV) with double spherical aberration correctors was used to investigate the electrochemical reactions of the gold anode. STEM-HAADF and STEM-ABF images were obtained at the collector angles of 100–267 and 11–22 mrad, respectively. To minimize the possible influence of electron irradiation, a short dwell time of 5 µs per pixel and a low magnification of 20–100K were used during operando STEM observations. At the low-dose STEM mode, the electron beam current is about 50 pA and the electron dose is ≤2.14 e^{-} $Å^{-2}$ (see the Supporting Information), which is about 4–5 orders of magnitude lower than that of the conventional TEM (≈10^5 e^{-} $Å^{-2}$).[38] The recorded images have the resolution of 512 by 512 pixels. A real-time video of the electrochemical reactions was record at ≈0.76 frame per second. In comparison with liquid-cell TEM, the Cs-corrected liquid-cell STEM provides a better spatial resolution and mass-sensitive contrast for imaging SEI films formed in the 200-nm-thick electrolyte surroundings. The calibrated spatial resolution of the liquid-cell STEM is better than 1.0 nm, which provides a sufficiently spatial resolution to resolve the kinetic process of SEI films and Li–Au reactions upon charge and discharge.

Supporting Information

Supporting Information is available from the Wiley Online Library or from the author.

Acknowledgements

This work was supported by MOST 973 of China (2015CB856800) and Natural Science Foundation of China (Grant Nos. 51821001, 11704245). P.L. is supported by the Program for Professor of Special Appointment (Eastern Scholar) at Shanghai Institutions of Higher Learning. M.C. is sponsored by the Whiting School of Engineering, Johns Hopkins University.

Conflict of Interest

The authors declare no conflict of interest.

Keywords

liquid cell electron microscopy, lithium-ion batteries, lithium-metal batteries, scanning transmission electron microscopy, solid electrolyte interphase

Received: August 16, 2019
Revised: September 29, 2019
Published online: October 28, 2019

[1] X. B. Cheng, R. Zhang, C. Z. Zhao, F. Wei, J. G. Zhang, Q. Zhang, *Adv. Sci.* **2016**, *3*, 1500213.
[2] E. Peled, *J. Electrochem. Soc.* **1979**, *126*, 2047.
[3] E. Peled, S. Menkin, *J. Electrochem. Soc.* **2017**, *164*, A1703.
[4] A. Kushima, K. P. So, C. Su, P. Bai, N. Kuriyama, T. Maebashi, Y. Fujiwara, M. Z. Bazant, J. Li, *Nano Energy* **2017**, *32*, 271.
[5] W. Xu, J. Wang, F. Ding, X. Chen, E. Nasybulin, Y. Zhang, J. G. Zhang, *Energy Environ. Sci.* **2014**, *7*, 513.
[6] J. Wen, Y. Yu, C. Chen, *Mater. Express* **2012**, *2*, 197.
[7] Q. Zhang, X. Xiao, W. Zhou, Y. T. Cheng, M. W. Verbrugge, *Adv. Energy Mater.* **2015**, *5*, 1401398.
[8] A. J. Leenheer, K. L. Jungjohann, K. R. Zavadil, C. T. Harris, *ACS Nano* **2016**, *10*, 5670.
[9] J. Lei, L. Li, R. Kostecki, R. Muller, F. McLarnon, *J. Electrochem. Soc.* **2005**, *152*, A774.
[10] R. Bhattacharyya, B. Key, H. Chen, A. S. Best, A. F. Hollenkamp, C. P. Grey, *Nat. Mater.* **2010**, *9*, 504.
[11] S. Chattopadhyay, A. L. Lipson, H. J. Karmel, J. D. Emery, T. T. Fister, P. A. Fenter, M. C. Hersam, M. J. Bedzyk, *Chem. Mater.* **2012**, *24*, 3038.
[12] H. Cheng, C. B. Zhu, M. Lu, Y. Yang, *J. Power Sources* **2007**, *174*, 1027.
[13] M. Itagaki, N. Kobari, S. Yotsuda, K. Watanabe, S. Kinoshita, M. Ue, *J. Power Sources* **2004**, *135*, 255.
[14] R. L. Sacci, N. J. Dudney, K. L. More, L. R. Parent, I. Arslan, N. D. Browning, R. R. Unocic, *Chem. Commun.* **2014**, *50*, 2104.
[15] R. R. Unocic, X. G. Sun, R. L. Sacci, L. A. Adamczyk, D. H. Alsem, S. Dai, N. J. Dudney, K. L. More, *Microsc. Microanal.* **2014**, *20*, 1029.
[16] Z. Zeng, W. I. Liang, H. G. Liao, H. L. Xin, Y. H. Chu, H. Zheng, *Nano Lett.* **2014**, *14*, 1745.
[17] F. A. Soto, Y. Ma, J. M. Martinez de la Hoz, J. M. Seminario, P. B. Balbuena, *Chem. Mater.* **2015**, *27*, 7990.
[18] E. Peled, H. Straze, *J. Electrochem. Soc.* **1977**, *124*, 1030.
[19] E. Peled, D. Golodnitsky, G. Ardel, *J. Electrochem. Soc.* **1997**, *144*, L208.
[20] S. Wei, S. Choudhury, Z. Tu, K. Zhang, L. A. Archer, *Acc. Chem. Res.* **2018**, *51*, 80.
[21] J. A. Dawson, P. Canepa, T. Famprikis, C. Masquelier, M. S. Islam, *J. Am. Chem. Soc.* **2018**, *140*, 362.
[22] S. Shi, P. Lu, Z. Liu, Y. Qi, L. G. Hector Jr., H. Li, S. J. Harris, *J. Am. Chem. Soc.* **2012**, *134*, 15476.
[23] X. B. Cheng, R. Zhang, C. Z. Zhao, Q. Zhang, *Chem. Rev.* **2017**, *117*, 10403.
[24] X. H. Liu, L. Zhong, L. Q. Zhang, A. Kushima, S. X. Mao, J. Li, Z. Z. Ye, J. P. Sullivan, J. Y. Huang, *Appl. Phys. Lett.* **2011**, *98*, 183107.
[25] S. Tehuacanero-Cuapa, J. Reyes-Gasga, A. Rodríguez-Gómez, D. Bahena, I. Hernández-Calderón, R. García-García, *J. Appl. Phys.* **2016**, *120*, 164302.
[26] X. H. Liu, J. Y. Huang, *Energy Environ. Sci.* **2011**, *4*, 3844.
[27] C. Li, P. Wang, S. Li, D. Zhao, Q. Zhao, H. Liu, X. Cui, *ACS Appl. Mater. Interfaces* **2018**, *10*, 25744.
[28] K. M. Reddy, P. Liu, A. Hirata, T. Fujita, M. W. Chen, *Nat. Commun.* **2013**, *4*, 2483.
[29] G. Liu, W. Lu, *J. Electrochem. Soc.* **2017**, *164*, A1826.
[30] M. Z. Winter, *Phys. Chem.* **2009**, *223*, 1395.
[31] K. Kanamura, H. Tamura, S. Shiraishi, Z. i. Takehara, *J. Electrochem. Soc.* **1995**, *142*, 340.
[32] Y. Ein-Eli, *Electrochem. Solid-State Lett.* **1999**, *2*, 212.
[33] W. Huang, P. M. Attia, H. Wang, S. E. Renfrew, N. Jin, S. Das, Z. Zhang, D. T. Boule, Y. Li, M. Z. Bazant, B. D. McCloskey, W. C. Chueh, Y. Cui, *Nano Lett.* **2019**, *19*, 5140.
[34] J. Zheng, M. Tang, Y. Y. Hu, *Angew. Chem., Int. Ed.* **2016**, *55*, 12538.
[35] X. B. Cheng, C. Yan, H. J. Peng, J. Q. Huang, S. T. Yang, Q. Zhang, *Energy Storage Mater.* **2018**, *10*, 199.
[36] M. B. Pinson, M. Z. Bazant, *J. Electrochem. Soc.* **2013**, *160*, A243.
[37] P. Liu, J. H. Han, X. W. Guo, Y. Ito, C. C. Yang, S. C. Ning, T. Fujita, A. Hirata, M. W. Chen, *Sci. Rep.* **2018**, *8*, 3134.
[38] J. P. Buban, Q. Ramasse, B. Gipson, N. D. Browning, H. J. Stahlberg, *J. Electron Microsc.* **2010**, *59*, 103.